The Journal of Chemical Physics

RESEARCH ARTICLE | JUNE 03 2025

Contact mechanics for layered materials: Rubber film on hard substrate

B. N. J. Persson

J. Chem. Phys. 162, 214702 (2025)
https://doi.org/10.1063/5.0274655

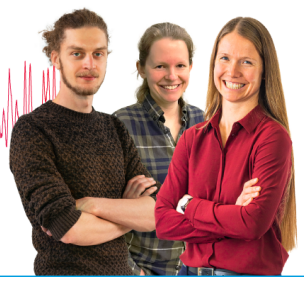

The Journal of Chemical Physics ARTICLE pubs.aip.org/aip/jcp

Contact mechanics for layered materials: Rubber film on hard substrate

Cite as: J. Chem. Phys. 162, 214702 (2025); doi: 10.1063/5.0274655
Submitted: 7 April 2025 • Accepted: 15 May 2025 •
Published Online: 3 June 2025

B. N. J. Persson[a)]

AFFILIATIONS

Peter Grünberg Institute (PGI-1), Forschungszentrum Jülich, 52425 Jülich, Germany; State Key Laboratory of Solid Lubrication, Lanzhou Institute of Chemical Physics, Chinese Academy of Sciences, 730000 Lanzhou, China; and MultiscaleConsulting, Wolfshovener str. 2, 52428 Jülich, Germany

[a)]Author to whom correspondence should be addressed: b.persson@fz-juelich.de

ABSTRACT

I consider the contact mechanics for a layered material, consisting of an elastically soft film glued to a hard substrate. I calculate the area of real contact for surfaces with fractal-like roughness and for surfaces with roughness in narrow length scale regions. For the fractal-like surfaces, when the product $q_0 d$ of the film thickness d and the low cut-off wavenumber q_0 of the surface roughness power spectrum satisfy $q_0 d < 0.1$, the effective modulus becomes very large. This results in large contact stresses, which can induce plastic deformation or wear, in particular during sliding contact. I also calculate the probability distributions of the normal and tangential stresses at the film–substrate interface. If the tangential (shear) stress is too high, the adhesive bond between the film and the substrate will break. I compare the thin-film contact mechanics problem with the Gent solution for a thin elastic sheet confined between two flat solid surfaces, and discuss the origin of the difference in effective elastic modulus.

I. INTRODUCTION

Thin coatings or films are used for many purposes such as paints for protection and aesthetic reason, or thin Teflon films on rubber for lowering the friction, or to reduce the migration of toxic (leachable) components from the rubber stopper to the fluid (drug) in syringes. In many applications, soft coatings such as rubber are used on steel surfaces as protection or to prevent (or reduce) marine growth and corrosion.

While thin coatings or films can have many beneficial effects, there are also several problems. For example, thin (~10 μm) Teflon coatings on rubber stoppers require extremely smooth surfaces to avoid leakage and to ensure microbial integrity. This is a consequence of the elastic modulus of the Teflon being ~1000 higher than for rubber, and therefore, even if the film is very thin, it cannot always deform enough at the interface for the contact area to percolate.[1,2]

A large number of papers have been published about various aspects of contact mechanics for layered materials.[3–8] In this report, we are interested in rubber coatings on hard countersurfaces, such as steel, which has a large number of practical applications. In most applications, the rubber films are strongly bound to the substrate, e.g., strong chemical bonds to brass or copper form if the rubber is vulcanized in contact with these metals (rubber molecules form covalent C–S–Cu bonds with the substrate). In some cases such as for silicone elastomer, strong covalent bonding to metals requires the use of a primer. In other cases, adhesives such as cyanoacrylate are used to form strong bonding between rubber and metals. In all these cases, describing the interfacial contact with a sliding friction coefficient is not appropriate, but the information about the shear stress acting between the rubber and countersurface in asperity contact regions is important for deciding if the adhesive bond will fail.

Since all surfaces have surface roughness, it is important to understand how roughness at different length scales affects the contact mechanics. We will show that with respect to short wavelength roughness, with a wavelength smaller than the thickness of the rubber film, the rubber deforms as a soft material; however, for the long-wavelength components, the effective modulus may be ~10^3 or more higher than the rubber bulk Young's modulus. As a result, during sliding contact, very high shear stresses may act on the rubber surface, which could result in damage to the rubber film, or break the adhesive bond between the rubber film and the contersurface.

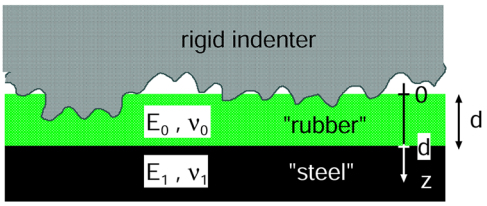

FIG. 1. A "steel" surface with a thin "rubber" film of thickness d.

II. THEORY

We consider a thin rubber film glued to a steel surface, see Fig. 1. The rubber film has uniform thickness but with roughness reflecting the roughness of the steel substrate. We present numerical results below assuming surfaces with two types of random roughness, but all with the root-mean-square slope $\xi = 1$.

When a rigid flat surface is squeezed against a homogeneous elastic solid (Young's modulus E and Poisson ratio ν), for small enough applied nominal contact pressure p_0, the area of real contact is given by[9–18]

$$\frac{A}{A_0} \approx \frac{\kappa p_0}{\xi E^*}, \tag{1}$$

where A_0 is the nominal contact area, $E^* = E/(1-\nu^2)$, and κ is a number of order 2.

We consider two types of roughness, namely, self-affine fractal surfaces (without roll-off), and surfaces with roughness only in a narrow range of length scales. The self-affine fractal surfaces have the surface roughness power spectra

$$C(q) = C_0 \left(\frac{q}{q_0}\right)^{-2(1+H)}, \tag{2}$$

for $q_0 < q < q_1$. We choose $q_1 = 10^8$ m^{-1} but vary the small wavenumber cut-off q_0 and choose C_0 so the rms slope $\xi = 1$ for all the surfaces.

The latter type of surfaces have roughness only in a small length scale region. We refer to this roughness as "waviness." A surface with roughness on a single-length scale can be obtained as the sum of roughness components,

$$h(\mathbf{x}) = a \cos(\mathbf{q}_0 \cdot \mathbf{x} + \phi_q),$$

where $\mathbf{q}_0$ is the random direction of the wave vector and ϕ_q is the random phase, with a and $|\mathbf{q}_0| = q_0$ being constant. Such surfaces will have surface roughness power spectra, which only depend on the magnitude q of the wave vector $\mathbf{q}$. It is intuitively plausible that such surfaces will have the power spectrum (see Appendix A for the proof),

$$C(q) = \alpha \delta(q - q_0).$$

If h_0^2 is the mean square (ms) roughness, then

$$h_0^2 = \int d^2q\, C(q) = 2\pi \int_0^\infty dq\, q\alpha\delta(q-q_0) = 2\pi\alpha q_0,$$

so that $\alpha = h_0^2/2\pi q_0$ and

$$C(q) = \frac{h_0^2}{2\pi q_0}\delta(q - q_0). \tag{3}$$

Note that the ms slope is

$$\xi^2 = \int d^2q\, q^2 C(q) = (h_0 q_0)^2. \tag{4}$$

In the numerical simulations presented below, we broaden the $\delta(q-q_0)$, which also makes the power spectrum more realistic as one seldom will have long wavelength roughness (waviness) involving just one length scale defined by q_0. We use the Gaussian approximation of the Dirac delta function,

$$\delta(q - q_0) \to \frac{1}{Q\sqrt{(2\pi)}} e^{-(q-q_0)^2/2Q^2},$$

where Q is the Gaussian root-mean-square (rms) width. The Dirac delta function is obtained from the limit $Q \to 0$. Thus, as the second type of power spectrum, we use

$$C(q) = \frac{h_0^2}{q} \frac{1}{Q(2\pi)^{3/2}} e^{-(q-q_0)^2/2Q^2}. \tag{5}$$

We will show the results for several values of q_0, and we always assume $Q = 0.1q_0$. Figure 2 shows a topography picture of a surface with the power spectrum [Eq. (5)], generated as described in Ref. 19 (Appendix A) by adding plane waves with random phases as in Eq. (A1). The surface has roughness in a very narrow length scale region, with a Gaussian height probability distribution. Incidentally, we note that it is only for surfaces of the type shown in Fig. 2, with roughness on a narrow length scale region, that the Greenwood–Williamson contact mechanics theory is (approximately) valid, assuming so low contact pressures that the elastic interaction between the asperities can be neglected.

In the numerical study, we use the Persson contact mechanics theory[9] and include layering as described in Ref. 4. Specifically, the response function M_{zz}, which enters in the Persson contact mechanics theory takes, for layered materials, the following form:

$$M_{zz}(q) = -\frac{2}{qE_0^*} S(q), \tag{6}$$

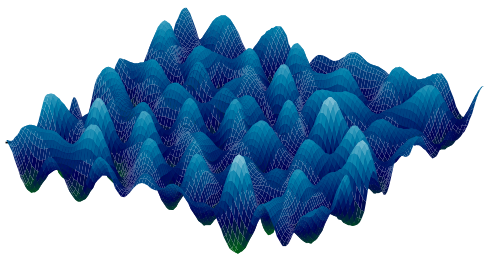

FIG. 2. A topography picture of a surface with the power spectrum (5). The surface has roughness in a very narrow length scale region. The height probability distribution is Gaussian.

where $E_0^* = E_0/(1-\nu_0^2)$ is the effective modulus of the top layer. For the case of one layer (thickness d) on top of a semi-infinite bulk with the modulus E_1 and the Poisson ratio ν_1, one has

$$S(q) = \frac{1 + 4mqde^{-2qd} - mne^{-4qd}}{1 - [m + n + 4m(qd)^2]e^{-2qd} + mne^{-4qd}}, \tag{7}$$

where

$$m = \frac{G_0/G_1 - 1}{G_0/G_1 + 3 - 4\nu_0},$$

$$n = 1 - \frac{4(1-\nu_0)}{1 + (G_0/G_1)(3-4\nu_1)},$$

where $G = E/2(1+\nu) = E/3$ for $\nu = 0.5$ is the shear modulus.

III. NUMERICAL RESULTS

To illustrate how roughness on different length scales influences contact mechanics, we consider first the Gaussian power spectra centered at different wavenumbers q_0. In all cases, we choose the rms roughness h_0 so that the rms surface slope $\xi = 1$. For a homogeneous solid, the contact area should be the same, independent of q_0, and given by (1) if $p_0/E^* \ll 1$. In this study, we use $p_0 = 0.1$ MPa so this condition is satisfied for the rubber (and, of course, for the steel).

In the numerical calculation, we denote the substrate as "steel" with Young's modulus and Poisson ratio $E_S = 10^{11}$ Pa and $\nu_S = 0.5$, respectively. The film on top is denoted as "rubber" with the elastic parameters $E_R = 10^6$ Pa and $\nu_R = 0.5$. The rubber film is $d = 50$ μm thick.

The blue lines in Fig. 3 show two Gaussian power spectra centered at $q_0 = 10^3$ and 10^5 m^{-1}. Both power spectra correspond to surfaces similar to those in Fig. 2 with the rms slope $\xi = 1$.

The blue line in Fig. 4 shows the normalized contact area A/A_0 as a function of the center wavenumber q_0 of the Gaussian power spectra. Note that the contact area of the homogeneous rubber and steel materials becomes $q_0 d \to \infty$ and 0, respectively. While the rubber limit is obtained for $q_0 d \gtrsim 5$, the steel limit is obtained only when $q_0 d \lesssim 0.005$.

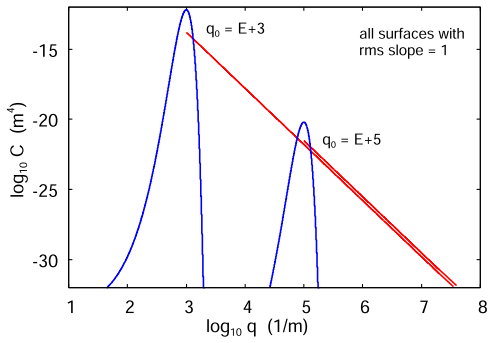

FIG. 3. Two power spectra for the fractal surface (red lines), and for the surface with a Gaussian power spectra (blue lines). The Hurst exponent of the fractal surface $H = 1$ and the rms width of the Gaussian is $q_0/10$. In the case of the fractal surfaces, the two low wavenumber cut-offs are $q_0 = 10^3$ and $q_0 = 10^5$ m^{-1}. The two Gaussian power spectra are centered at the same two values for q_0.

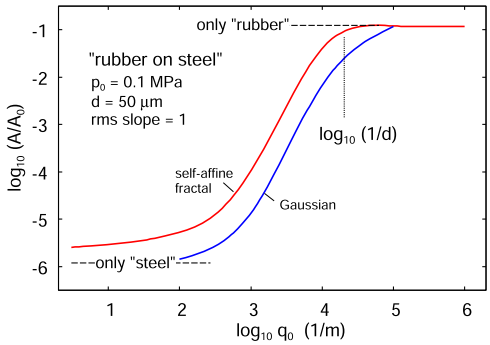

FIG. 4. The normalized contact area A/A_0 as a function of the cut-off wavenumber q_0 (for the fractal surfaces) or center wavenumber q_0 (for the Gaussian power spectra). All surfaces have the rms slope $\xi = 1$.

We have also performed calculations for a more realistic fractal-like surface with the Hurst exponent $H = 1$ and the large wavenumber cut-off $q_1 = 10^8$ m^{-1}. We have varied the low wavenumber cut-off q_0 and chosen the rms roughness h_0 so that the rms slope $\xi = 1$ for all surfaces. The two red lines in Fig. 3 show the power spectra for $q_0 = 10^3$ and 10^5 m^{-1}.

The red line in Fig. 4 shows the normalized contact area A/A_0 as a function of the center wavenumber q_0 of the fractal-like power spectra. Note that the contact area approach that of the homogeneous rubber and steel materials as $q_0 d \to \infty$ and 0, respectively. While the rubber limit is obtained for $q_0 d \gtrsim 2$, the steel limit is obtained only for extremely small $q_0 d$.

Real rubber materials are not incompressible and, thus, have Poisson ratios slightly smaller than 0.5. The bulk modulus of rubber is similar to that of other polymers and is typically $K_R \approx 2 \times 10^9$ Pa. (Most materials have a similar bulk modulus as Young's modulus; however, this is not the case for rubber because its Young's modulus is of entropic origin, whereas its bulk modulus is determined by compression of molecular chains interacting with the van der Waals interaction and the short ranged Pauli repulsion.) Assuming the rubber's bulk modulus $K_R \approx 2 \times 10^9$ Pa and Young's modulus $E_R = 2 \times 10^6$ Pa as in the calculations above, and using $E = 3K(1-2\nu)$, we get $\nu_R \approx 0.499\,85$. In Fig. 5, we compare the result for A/A_0 as a function of q_0 calculated with $\nu \approx 0.499\,85$ (green curve) with the results for $\nu_R = 0.5$ (red curve, from Fig. 4). Clearly, the difference between the two curves is negligible for all values of q_0.

The theory presented in Ref. 4 and in Appendix B also predicts the normal and the shear stress at the interface between the rubber film and the steel surface. I note that Johnson[20] and Barber[21] have also studied the stress at interfaces of layered materials, but only for smooth surfaces with different macroscopic curvatures. However, all real surfaces have random roughness on many length scales, which is a topic much more complex than for smooth curved surfaces. In addition, Johnson and Barber assumed that the contact between the film and the substrate can be described using friction coefficients,

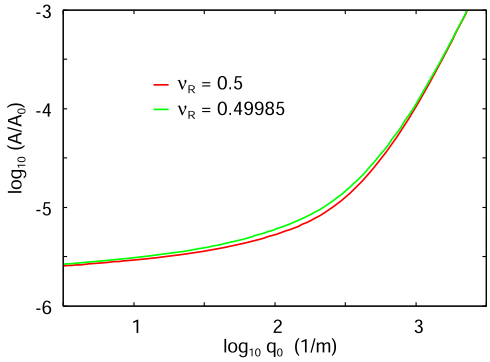

FIG. 5. The normalized contact area A/A_0 as a function of the cut-off wavenumber q_0 for the fractal-like surfaces for the rubber Poisson ratio $\nu_R = 0.5$ (red line) and $\nu_R = 0.499\,85$ (green line). All surfaces have the rms slope $\xi = 1$.

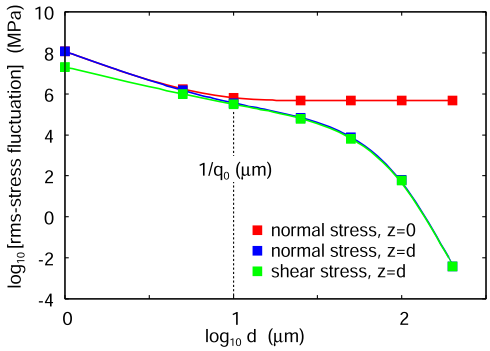

FIG. 7. The rms width of the stress probability distributions as a function of the film thickness (log–log scale), for the fractal-like surface with $q_0 = 10^5\ \mathrm{m}^{-1}$.

which is not the case if the film is glued, or bonded by covalent bonds, to the substrate.

If the normal stress is too high, it could plastically deform the steel (or other softer substrate material); if the shear stress is too high, it can break the adhesive bond between the rubber and the steel surface. For rubber glued to the steel surface using, e.g., epoxy resin, tearing experiments show that the adhesive bond breaks at a typical shear stress of ~10 MPa. Because of the random nature of surface roughness, the stress at the rubber–steel interface will not be uniform and can only be characterized by probability distributions. Using the theory of Ref. 4, one can obtain the distributions of normal stress $P(\sigma)$ and shear stress $P(\tau)$. Using the equations summarized in Appendix B, we show in Fig. 6 the probability distribution of normal stress $P(\sigma)$ at the upper surface (red curve) and at the steel–rubber interface (blue curve). The green curve shows the distribution $P(\tau)$ of shear stress. All probability distributions are normalized so that

$$\int_0^\infty d\sigma\ P(\sigma) = 1, \qquad \int_{-\infty}^\infty d\tau\ P(\tau) = 1.$$

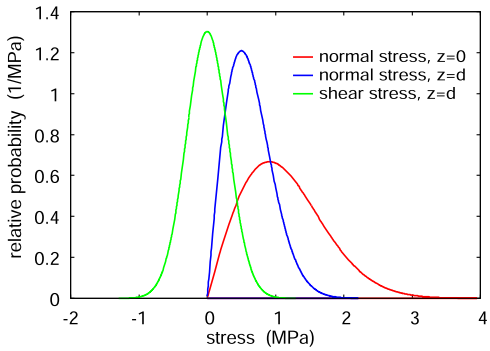

FIG. 6. The relative probabilities to find normal stress σ at the top surface ($z = 0$) (red line) and at the interface $z = d$ (blue line), and the shear stress τ at the interface (green line), for the fractal-like surface with $q_0 = 10^5\ \mathrm{m}^{-1}$ and film thickness $d = 10\ \mu$m.

In the calculations, we assumed a $d = 10\ \mu$m thick rubber film and used the self-affine fractal surface with the low wavenumber cut-off $q_0 = 10^5\ \mathrm{m}^{-1}$.

In Fig. 7, the blue and green lines show for the same rough surface, the root-mean-square width of the probability distribution of normal stress and shear stress at the rubber–steel interface, as a function of the rubber film thickness (log–log scale). The red line shows the root-mean-square width of the probability distribution at the top surface of the rubber film. Note that, for a large rubber film thickness, the normal stress and the shear stress exhibit the same stress fluctuations and that, for $d \gg 1/q_0$, the stress fluctuations at the interface become very small so that $\tau \approx 0$ and $\sigma \approx \sigma_0$. The physical reason for this is illustrated schematically in Fig. 8 for the contact between a rubber film and a randomly rough surface with short-wavelength roughness $q_0 d \gg 1$ [Fig. 8(a)] and long-wavelength roughness $q_0 d \ll 1$ [Fig. 8(b)]. For large film thickness $q_0 d \gtrsim 2$, the width of the stress distribution at the top of the film ($z = 0$) is constant, which indicates that the film with respect to the stress at this surface can already be considered as infinite thick when $q_0 d \gtrsim 2$. For small film thickness, the normal stress at the interface is nearly the same as at the top surface (red and blue lines for

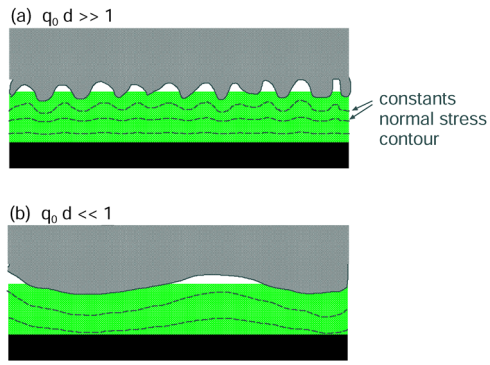

FIG. 8. The contact between a rubber film and a randomly rough surface with (a) short-wavelength roughness, $q_0 d \gg 1$ and (b) long-wavelength roughness $q_0 d \ll 1$ (schematic).

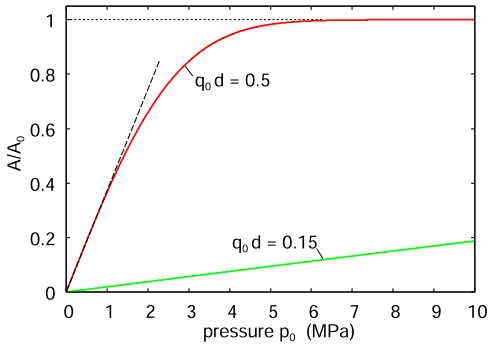

FIG. 9. The normalized contact area A/A_0 as a function of the squeezing pressure p_0 for the cut-off wavenumbers q_0 (for the fractal surfaces) $q_0 = 10^4$ m^{-1} (red curve) and 3×10^3 m^{-1} (green curve).

$q_0 d \lesssim 1/2$), while the shear stress increases more slowly than the normal stress with decreasing film thickness.

Rubber coating on steel has a typical thickness of 50–500 μm. Most surfaces in engineering applications have the cut-off (or rather roll-off) wavenumber $q_0 \approx 10^5$ m^{-1} so that $q_0 d$ is typically in the range of 5–50. For this large $q_0 d$, the shear stress at the steel–rubber interface is already strongly reduced from what is expected for $q_0 d < 1$ and the shear stress in most cases will be well below the yield limit where the stress can break the adhesive bond between the rubber film and the steel surface. This conclusion holds for stationary contact, but during sliding, larger shear stresses may prevail but this topic will not be addressed here.

IV. DISCUSSION AND CONCLUSION

When the roughness wavelength is much larger than the thickness of the rubber film, the film behaves as an elastically very stiff material. Nevertheless, the contact area depends linearly on the applied pressure p_0 for low enough pressures (see Fig. 9), and one can define an effective modulus E_{eff} that depends on the low wavenumber cut-off q_0 and the film thickness d. As $q_0 d \to 0$, we must have $E_{\text{eff}} \to E_S$, and as $q_0 d \to \infty$, we must have $E_{\text{eff}} \to E_R$. In

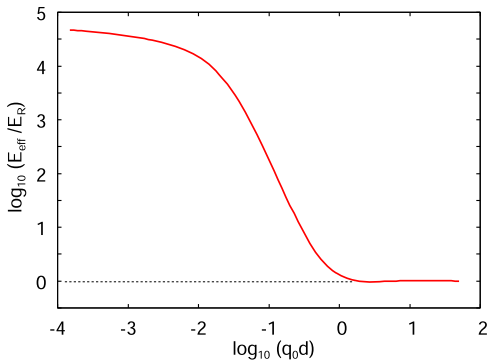

FIG. 10. The effective modulus E_{eff} normalized by the modulus of the rubber and E_R as a function of $q_0 d$ (log–log scale), for the fractal surfaces with the power spectrum (2).

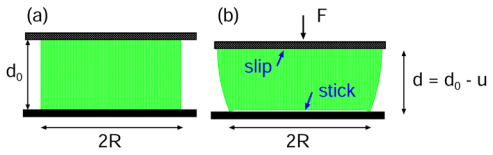

FIG. 11. A cylindrical block with radius R and height d_0 is squeezed between two rigid plates. At the lower plate, no slip occurs, while the upper interface is lubricated and slip occurs so that the shear stress vanishes. For an incompressible material, the relation between the displacement u and the squeezing force F can, for $u \ll d_0$, be approximately obtained by considering the solid as a very high viscosity fluid (viscosity η) with the shear modulus $G(\omega) = -i\eta\omega$ (see Appendix C).

Fig. 10, we show E_{eff}/E_R as a function of $q_0 d$ for the fractal-like surface with the power spectra (2).

A similar contact mechanics effect as described above, and of the same origin, is observed in the compression of a rubber block against a rigid surface assuming no slip at the bottom interface (see Fig. 11). This topic was studied by Gent.[22–25] He used a method now denoted the "pressure method" [in Appendix C, we present a slightly different (and simpler) derivation of the Gent result]. Gent showed that there is a compressive pressure in the film $p = 2p_0[1 - (r/R)^2]$, where $p_0 = F/\pi R^2$ is the average squeezing pressure, and that the compressive strain $\epsilon = u/d$ is related to the applied (average) pressure p_0 as

$$p_0 = E_{\text{eff}}\epsilon$$

with

$$E_{\text{eff}} \approx \frac{1}{8}\left(\frac{R}{d}\right)^2 E_R. \tag{8}$$

For $d \gg R$, we have $E_{\text{eff}} \approx E_R$, and we can interpolate between this limit and (8) using

$$\frac{E_{\text{eff}}}{E_R} \approx 1 + \frac{1}{8}\left(\frac{R}{d}\right)^2. \tag{9}$$

We can compare this prediction with the results presented above for the Gaussian roughness case. In Fig. 12, we show the

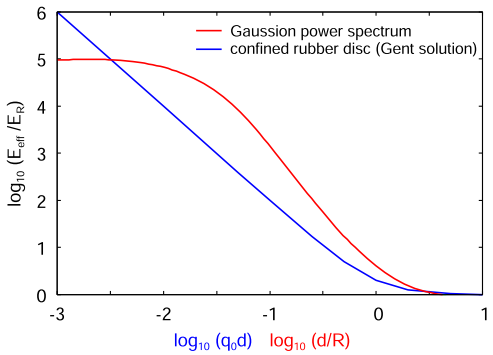

FIG. 12. The effective Young's modulus for the roughness with Gaussian power spectrum and the confined cylinder disc in Fig. 11 [Eq. (9)] as a function of $q_0 d$ and d/R, respectively (log–log scale). For the Gaussian power spectrum case, we have varied d but kept $q_0 = 10^5$ m^{-1} fixed.

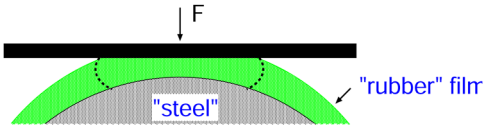

FIG. 13. The deformation at contact between an asperity and a flat surface for the case of the Gaussian power spectrum. The dashed lines indicate how the rubber at the edge of the contact bends outwards, but this bending is resisted by the rubber film outside of the contact region. This differs from the cylinder disc case in Fig. 11, where there is nothing "outside" resisting the bending.

effective Young's modulus for the roughness with Gaussian power spectrum and for the confined cylinder disc in Fig. 11, as a function of $q_0 d$ and d/R, respectively (log–log scale). Note that, for the Gaussian case, for $q_0 d > 0$, before saturating for small $q_0 d$ at E_S/E_R, the effective modulus increases faster with decreasing film thickness than for the confined rubber cylinder disc in Fig. 11. This can be understood as follows.

For the rough surface, the roughness profile consists of spherical cup-like bumps (see Fig. 2). When a bump is squeezed against a flat rigid surface, the rubber at the edge of the contact bends outward (dashed lines in Fig. 13); however, this bending is resisted by the rubber film outside of the contact region (see Fig. 13). This differs from the cylinder disc case in Fig. 11, where the nothing "outside" resists the bending. This additional confinement results in a faster increase in the E_{eff}/E_R with decreasing thickness d for the film, as compared to the disc.

In the calculations, we have used a relatively small nominal contact pressure $p_0 = 10^5$ Pa. The average pressure in the area of real contact equals $p = p_0 A_0/A$. Figure 4 shows that for surfaces with long wavelength roughness $\lambda_0 \gg d$ or $q_0 d \ll 1$, this pressure can be extremely large approaching that expected for a material with the elastic modulus of steel where $A/A_0 \approx 2p_0/\xi E_S^*$ so that $p \approx \xi E_S^*/2$. In practice, this high pressure cannot be reached since steel yields plastically at much lower contact pressures (typically a few GPa). Furthermore, during slip, very high frictional stress will act on the rubber film, which may break the rubber–steel adhesive bond. We note that the "dangerous" roughness components are those with wavelengths longer than the rubber film thickness so the long-wavelength "waviness" should be small in order to avoid large contact stresses.

AUTHOR DECLARATIONS

Conflict of Interest

The author has no conflicts to disclose.

Author Contributions

B. N. J. Persson: Conceptualization (equal); Data curation (equal); Formal analysis (equal); Funding acquisition (equal); Investigation (equal); Methodology (equal); Project administration (equal); Resources (equal); Software (equal); Supervision (equal); Validation (equal); Visualization (equal); Writing – original draft (equal); Writing – review & editing (equal).

DATA AVAILABILITY

The data that support the findings of this study are available within the article.

APPENDIX A: SURFACE ROUGHNESS POWER SPECTRA FOR A SURFACE WITH ROUGHNESS IN A NARROW LENGTH SCALE REGION

The result (3) can be proved as follows. We write the height field as

$$h(\mathbf{x}) = \sum_{\mathbf{q}'} a \cos(\mathbf{q}' \cdot \mathbf{x} + \phi_{\mathbf{q}'}), \tag{A1}$$

where a is a constant, the sum is over the different direction of the wavevector but with the same magnitude $|\mathbf{q}'| = q_0$, and the phases $\phi_{\mathbf{q}'}$ are random numbers uniformly distributed between 0 and 2π. Using the definition,

$$C(\mathbf{q}) = \frac{1}{(2\pi)^2} \int d^2q \langle h(\mathbf{x}) h(\mathbf{0}) \rangle e^{i\mathbf{q}\cdot\mathbf{x}},$$

and that

$$\begin{aligned} \langle \cos(\mathbf{q}' \cdot \mathbf{x} + \phi_{\mathbf{q}'}) \cos(\phi_{\mathbf{q}''}) \rangle &= \frac{1}{2} \langle \cos(\mathbf{q}' \cdot \mathbf{x} + \phi_{\mathbf{q}'} + \phi_{\mathbf{q}''}) \\ &\quad + \cos(\mathbf{q}' \cdot \mathbf{x} + \phi_{\mathbf{q}'} - \phi_{\mathbf{q}''}) \rangle \\ &= \frac{1}{2} \delta_{\mathbf{q}'\mathbf{q}''} \cos(\mathbf{q}' \cdot \mathbf{x}), \end{aligned}$$

we get

$$\begin{aligned} C(\mathbf{q}) &= \frac{1}{(2\pi)^2} \frac{a^2}{2} \sum_{\mathbf{q}'} \int d^2x \cos(\mathbf{q}' \cdot \mathbf{x}) e^{i\mathbf{q}\cdot\mathbf{x}} \\ &= \frac{a^2}{8\pi} \sum_{\mathbf{q}'} [\delta(\mathbf{q} + \mathbf{q}') + \delta(\mathbf{q} - \mathbf{q}')]. \end{aligned}$$

Both terms in this expression are identical so that

$$C(\mathbf{q}) = \frac{a^2}{4\pi} \sum_{\mathbf{q}'} \delta(\mathbf{q} + \mathbf{q}'). \tag{A2}$$

In the continuum limit, the sum over the direction of the wavevector $\mathbf{q}' = q_0(\cos\theta, \sin\theta)$ can be written as

$$\int_0^{2\pi} d\theta = \int d^2q' \frac{1}{q'} \delta(q' - q_0).$$

Using this result in (A2) gives

$$C(\mathbf{q}) = \frac{a^2}{4\pi} \int d^2q' \frac{1}{q'} \delta(q' - q_0) \delta(\mathbf{q} + \mathbf{q}') = \frac{a^2}{4\pi q} \delta(q - q_0).$$

We can choose a so that the mean square amplitude becomes h_0^2, which gives (3).

APPENDIX B: BASIC EQUATIONS FOR THE RMS WIDTH OF STRESS FLUCTUATIONS

Here, we derive the probability distributions of the shear stress and the normal stress at the steel-rubber interface. The results are based on the equations derived in Ref. 4. Although we are interested in static contact in the present approach (see Ref. 4), it is necessary to assume a small finite frequency ω, which is chosen so small that the final result does not depend on ω.

Let $\mathbf{n}$ denote the normal to the surface at the interface, and let z be a coordinate axis along $\mathbf{n}$ with a positive direction into the solid. The Fourier transform of the stress $\sigma_{ij}n_j$ at the interface can be written as

$$\sigma_{\rm n}\mathbf{n} + \hat{q}\sigma_{\mathbf{q}},$$

where $\hat{q} = \mathbf{q}/q$ is a unit vector along the wavevector $\mathbf{q}$. Using (3), (5), (26), and (27) in Ref. 4, we get

$$\frac{-i}{\mu_0}\sigma_{\rm n} = Rq^2A_0\left(e^{-ip_{\rm L}d} + r_Ae^{ip_{\rm L}d}\right) + 2q^2(-iq\tilde{p}_T)C_0\left(e^{-ip_{\rm T}d} - r_Ce^{ip_{\rm T}d}\right), \tag{B1}$$

$$\frac{-i}{\mu_0}q\sigma_{\mathbf{q}} = 2q^2(-iq\tilde{p}_{\rm L})A_0\left(e^{-ip_{\rm L}d} - r_Ae^{ip_{\rm L}d}\right) - q^4RC_0\left(e^{-ip_{\rm T}d} + r_Ce^{ip_{\rm T}d}\right), \tag{B2}$$

where

$$R = \left(\frac{\omega}{qc_{\rm T}}\right)^2 - 2,$$

and $p_{\rm L} = -iq\tilde{p}_{\rm L}$, $p_{\rm T} = -iq\tilde{p}_{\rm T}$, with

$$\tilde{p}_{\rm L} = \left[1 - \left(\frac{\omega}{qc_{\rm L}}\right)^2\right]^{1/2}, \qquad \tilde{p}_{\rm T} = \left[1 - \left(\frac{\omega}{qc_{\rm T}}\right)^2\right]^{1/2}.$$

The condition (31) in Ref. 4 gives

$$\frac{A_0}{C_0} = -\frac{Rq}{2i\tilde{p}_{\rm L}}\frac{1+r_C}{1-r_A}. \tag{B3}$$

Using (B1) and (B3) gives

$$\frac{1}{\mu_0q^3C_0}\sigma_{\rm n} = -\frac{R^2}{2\tilde{p}_{\rm L}}\frac{1+r_C}{1-r_A}\left(e^{-ip_{\rm L}d} + r_Ae^{ip_{\rm L}d}\right) + 2\tilde{p}_{\rm T}\left(e^{-ip_{\rm T}d} - r_Ce^{ip_{\rm T}d}\right). \tag{B4}$$

If $\sigma_{\rm n0}$ denotes the stress at the upper surface $z = 0$, we get from (B4) with $d = 0$

$$\frac{1}{\mu_0q^3C_0}\sigma_{\rm n0} = -\frac{R^2}{2\tilde{p}_{\rm L}}\frac{1+r_C}{1-r_A}(1+r_A) + 2\tilde{p}_{\rm T}(1-r_C). \tag{B5}$$

Using (B2) and (B3) gives

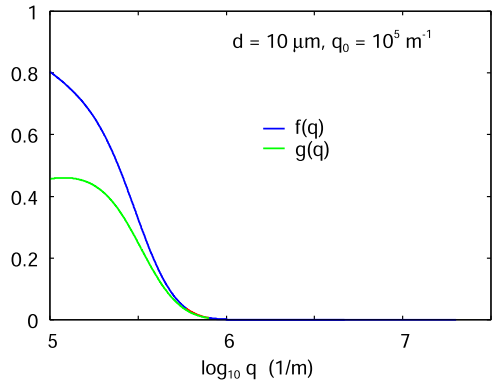

FIG. 14. The ratio $f(qd) = \sigma_{\rm n}(q,d)/\sigma_{\rm n}(q,0)$ between the Fourier transform of the normal stress at the interface $z = d$ and at the surface $z = 0$ as a function of the wavenumber, and the ratio $g(qd) = -i\sigma_q(q,d)/\sigma_{\rm n}(q,0)$ between the Fourier transform of the shear stress σ_q (which is along the direction of the wavevector $\mathbf{q}$) at the interface $z = d$ and the normal stress at the surface $z = 0$ as a function of the wavenumber, for the self-affine fractal surface with $q_0 = 10^5$ m^{-1} and the film thickness $d = 10$ μm.

$$\frac{-i}{\mu_0q^3C_0}\sigma_{\mathbf{q}} = R\frac{1+r_C}{1-r_A}\left(e^{-ip_{\rm L}d} - r_Ae^{ip_{\rm L}d}\right) - R\left(e^{-ip_{\rm T}d} + r_Ce^{ip_{\rm T}d}\right). \tag{B6}$$

We define

$$f(qd) = \frac{\sigma_{\rm n}}{\sigma_{\rm n0}}, \qquad g(qd) = \frac{-i\sigma_{\mathbf{q}}}{\sigma_{\rm n0}}, \tag{B7}$$

which are obtained using (B4)–(B6) and are function of qd. Figure 14 shows $f(qd)$ and $q(qd)$ for a 10 μm thick rubber film on steel. The surface roughness has the long wavelength cut-off wavenumber $q_0 = 10^5$ m^{-1}. Note that $f(qd)$ and $g(qd)$ are non-zero only for small wavenumbers because only the long wavelength (or small wavenumber) part of the pressure at $z = 0$ can give rise to stress fluctuations at the rubber-steel interface ($z = d$) as illustrated in Fig. 8.

The normal stress probability distribution $P(u)$ at the surface $z = 0$ is centered at the applied nominal contact pressure σ_0 and is given by the Persson contact mechanics theory. The normal stress at the rubber–steel interface has a similar form but with a smaller width. The shear stress probability distribution $P(\tau)$ is assumed to be Gaussian and centered at $\tau = 0$, since the average shear stress must vanish by symmetry, see Fig. 6. To calculate the rms width of the distributions, we use the equation (see Ref. 26)

$$\langle(\sigma - \sigma_0)^2\rangle = \frac{(2\pi)^2}{A_0}\int d^2q\,|\sigma(\mathbf{q})|^2,$$

where the stress $\sigma(\mathbf{q})$ could be either $\sigma_{\rm n}$ or (with $\sigma_0 = 0$) $\sigma_{\mathbf{q}}$. Using (B7), we get

$$\langle(\sigma - \sigma_0)^2\rangle = \frac{(2\pi)^2}{A_0}\int d^2q\,|f(qd)|^2|\sigma_{\rm n0}(\mathbf{q})|^2, \tag{B8}$$

$$\langle\tau^2\rangle = \frac{(2\pi)^2}{A_0}\int d^2q\,|g(qd)|^2|\sigma_{\rm n0}(\mathbf{q})|^2. \tag{B9}$$

For a layered material,

$$|\sigma_{n0}(\mathbf{q})|^2 = \left(\frac{E_0^*}{4\pi}\right)^2 A_0 q^2 C(q) S^{-2}(q) P(q), \tag{B10}$$

where $S(q)$ is given by (7) and

$$P(q) = \mathrm{erf}\left(\frac{\sigma_0}{2G^{1/2}}\right), \tag{B11}$$

with

$$G(q) = \frac{\pi}{4}(E_0^*)^2 \int_{q_0}^{q_1} dq\, q^3 C(q) S^{-2}(q). \tag{B12}$$

Using (B8)–(B12), we can calculate the rms stress fluctuations at the interface between the rubber and the steel surface. The results for a self-affine fractal surface with the cut-off $q_0 = 10^5\ \mathrm{m}^{-1}$ are shown in Fig. 7.

APPENDIX C: A NEW DERIVATION OF THE GENT EXPRESSION FOR THE COMPRESSED CONFINED RUBBER BLOCK

Gent derived (8) for incompressible solids using a method now denoted the "pressure method." In this method, the total displacement of a bounded rubber layer subject to uniform compression is composed of the superposition of two simple displacements: pure homogeneous compression between two flat walls with slip boundary conditions (no friction) and additional shear displacements to keep the bonded surfaces in their original positions. Here, we will treat the rubber film as a high-viscosity fluid (as would be the case if the rubber were uncrosslinked) and derive the same result using the standard fluid squeeze-out theory for fluids between a circular disc (radius R) and a flat substrate. This approach is based on the fact that, on short enough time scales, liquids can behave as solids (as for silica glass which behaves as a solid during fast deformation but flows as a fluid on very long time scales).

In this section, we denote the thickness of the solid (or fluid) film by h. We consider the case where the fluid sticks on the substrate surface (no-slip boundary condition) while the shear stress vanishes (slip without friction) on the disc surface. If $h(t)$ and $p(t)$ are the surface separation and average squeezing pressure at time t, respectively, then the Reynolds thin-film fluid flow equation gives the pressure distribution in the film

$$p(r,t) = 2p(t)\left[1 - \left(\frac{r}{R}\right)^2\right] \tag{C1}$$

and

$$\frac{dh}{dt} = -\frac{8h^3 p}{3\eta R^2}. \tag{C2}$$

For the case of a solid of undeformed width h_0, we write $h(t) = h_0[1 - \epsilon(t)]$ and assume that the strain $\epsilon(t) \ll 1$ so we can linearize (C2) to get

$$\frac{d\epsilon}{dt} = \frac{8h_0^2}{3\eta R^2} p(t).$$

If $p(t) = p(\omega)e^{-i\omega t}$ and $\epsilon(t) = \epsilon(\omega)e^{-i\omega t}$, then

$$-i\omega\epsilon(\omega) = \frac{8h_0^2 p(\omega)}{3\eta R^2}.$$

Using the shear modulus $G(\omega) = -i\omega\eta$, we can write

$$G(\omega)\epsilon(\omega) = \frac{8h_0^2 p(\omega)}{3R^2},$$

or

$$G\epsilon = \frac{8h_0^2 p}{3R^2}.$$

For an incompressible solid, $G = E/3$ giving

$$E_{\mathrm{eff}}\epsilon = p,$$

where

$$E_{\mathrm{eff}} = \frac{1}{8}\left(\frac{R}{h_0}\right)^2 E. \tag{C3}$$

In the limit $h \gg R$ (assuming no buckling), one must have $E_{\mathrm{eff}} = E_{\mathrm{R}}$ so that

$$E_{\mathrm{eff}} \approx E_{\mathrm{R}}\left[1 + \frac{1}{8}\left(\frac{R}{h}\right)^2\right]$$

is an interpolation formula approximately valid for all ratios h/R.

The same procedure as above gives for the case of stick boundary condition on both surfaces the same pressure profile (C1) but (C3) is replaced by

$$E_{\mathrm{eff}} = \frac{1}{2}\left(\frac{R}{h_0}\right)^2 E. \tag{C4}$$

REFERENCES

[1] N. Rodriguez, A. Tiwari, and B. N. J. Persson, "Air leakage in seals with application to syringes," Appl. Surf. Sci. Adv. **8**, 100222 (2022).

[2] T. Alexopoulos, E. N. Gazis, S. Maltezos, G. Koutelieris, and B. N. J. Persson, "On the use of foam rubber for sealing applications," Tribol. Lett. **72**, 39 (2024).

[3] P. M. McGuiggan, J. S. Wallace, D. T. Smith, I. Sridhar, Z. W. Zheng, and K. L. Johnson, "Contact mechanics of layered elastic materials: Experiment and theory," J. Phys. D: Appl. Phys. **40**, 5984 (2007).

[4] B. N. J. Persson, "Contact mechanics for layered materials with randomly rough surfaces," J. Phys. Condens. Matter **24**, 095008 (2012).

[5] Q. Dong, Y. Li, J. Wei, and F. Lu, "Layered structures with rough surfaces and interfaces at contact loading," Int. J. Mech. Sci. **178**, 105611 (2020).

[6] N. Menga, C. Putignano, L. Afferrante, and G. Carbone, "The contact mechanics of coated elastic solids: Effect of coating thickness and stiffness," Tribol. Lett. **67**, 24 (2019).

[7] M. Scaraggi and D. Comingio, "Rough contact mechanics for viscoelastic graded materials: The role of small-scale wavelengths on rubber friction," Int. J. Solids Struct. **125**, 276 (2017).

[8] A. Wang and M. H. Müser, "Percolation and Reynolds flow in elastic contacts of isotropic and anisotropic, randomly rough surfaces," Tribol. Lett. **69**, 1 (2021).

[9] B. N. J. Persson, "Theory of rubber friction and contact mechanics," J. Chem. Phys. **115**, 3840 (2001).

[10]S. Hyun, L. Pei, J. F. Molinari, and M. O. Robbins, Phys. Rev. E **70**, 026117 (2004).
[11]N. Prodanov, W. B. Dapp, and M. H. Müser, "On the contact area and mean gap of rough, elastic contacts: Dimensional analysis, numerical corrections, and reference data," Tribol. Lett. **53**, 433 (2014).
[12]C. Yang and B. N. J. Persson, "Contact mechanics: Contact area and interfacial separation from small contact to full contact," J. Phys.: Condens. Matter **20**, 215214 (2008).
[13]B. N. J. Persson, "Contact mechanics for randomly rough surfaces," Surf. Sci. Rep. **61**, 201 (2006).
[14]H. Terwisscha-Dekker, A. M. Brouwer, B. Weber, and D. Bonn, "Elastic contact between rough surfaces: Bridging the gap between theory and experiment," J. Mech. Phys. Solids **188**, 105676 (2024).
[15]F. Kaiser, D. Savio, and R. Bactavatchalou, "Modelling of static and dynamic elastomer friction in dry conditions," Lubricants **12**, 250 (2024).
[16]M. H. Müser, "How static is static friction?," Proc. Natl. Acad. Sci. U. S. A. **105**, 13187 (2008).
[17]S. Sills *et al.*, "Molecular origins of elastomeric friction, nanotribology," in *Friction and Wear on the Atomic Scale*, edited by E. Gnecco and E. Meyer (Springer Verlag, 2007), Chap. 30, pp. 659–676.
[18]B. N. J. Persson, I. M. Sivebaek, V. N. Samoilov, K. Zhao, A. I. Volokitin, and Z. Zhang, "On the origin of Amonton's friction law," J. Phys.: Condens. Matter **20**, 395006 (2008).
[19]B. N. J. Persson, O. Albohr, U. Tartaglino, A. I. Volokitin, and E. Tosatti, "On the nature of surface roughness with application to contact mechanics, sealing, rubber friction and adhesion," J. Phys.: Condens. Matter **17**, R1 (2004).
[20]K. L. Johnson, *Contact Mechanics* (Cambridge University Press, Cambridge, 1985).
[21]J. R. Barber, *Contact Mechanics* (Springer International Publishing, Basel, 2018).
[22]A. N. Gent and P. B. Lindley, "The compression of bonded rubber blocks," Proc. Inst. Mech. Eng. **173**, 111 (1959).
[23]A. N. Gent, "Compression of rubber blocks," Rubber Chem. Technol. **67**, 549 (1994).
[24]H. T. Banks, G. A. Pinter, and O. H. Yeoh, "Analysis of bonded elastic blocks," Math. Comput. Modell. **36**, 875 (2002).
[25]S. Polukoshko, V. Gonca, A. Martinovs, and S. Sokolova, "Boundary conditions influence on compressive stiffness of elastic isolators," Eng. Rural Dev. **25**, 737 (2016).
[26]B. N. J. Persson, "On the elastic energy and stress correlation in the contact between elastic solids with randomly rough surfaces," J. Phys.: Condens. Matter **20**, 312001 (2008).